Doping and critical-temperature dependence of the energy gaps in Ba(Fe_{1x}Co_{x})_{2}As_{2} thin films

Doping and critical-temperature dependence of the energy gaps in $Ba(Fe_{1-x}Co_x)_2As_2$ thin films

P. Pecchio, D. Daghero, G. A. Ummarino, and R. S. Gonnelli
Dipartimento di Scienza Applicata e Tecnologia, Politecnico di Torino, 10129 Torino, Italy

F. Kurth, B. Holzapfel, and K. Iida
Leibniz-Institut für Festkörper-und Werkstoffforschung (IFW) Dresden, P.O. Box 270116, 01171 Dresden, Germany
(Received 1 August 2013; revised manuscript received 22 October 2013; published 11 November 2013)

The dependence of the superconducting gaps in epitaxial $Ba(Fe_{1-x}Co_x)_2As_2$ thin films on the nominal doping x ($0.04 \leqslant x \leqslant 0.15$) was studied by means of point-contact Andreev-reflection spectroscopy. The normalized conductance curves were well fitted by using the two-dimensional Blonder-Tinkham-Klapwijk model with two nodeless, isotropic gaps—although the possible presence of gap anisotropies cannot be completely excluded. The amplitudes of the two gaps Δ_S and Δ_L show similar monotonic trends as a function of the local critical temperature T_c^A (measured in the same point contacts) from 25 K down to 8 K. The dependence of the gaps on x is well correlated to the trend of the critical temperature, i.e., to the shape of the superconducting region in the phase diagram. When analyzed within a simple three-band Eliashberg model, this trend turns out to be compatible with a mechanism of superconducting coupling mediated by spin fluctuations, whose characteristic energy scales with T_c according to the empirical law $\Omega_0 = 4.65 k_B T_c$, and with a total electron-boson coupling strength $\lambda_{tot} = 2.22$ for $x \leqslant 0.10$ (i.e., up to optimal doping) that slightly decreases to $\lambda_{tot} = 1.82$ in the overdoped samples ($x = 0.15$).

DOI: 10.1103/PhysRevB.88.174506 PACS number(s): 74.45.+c, 74.70.Xa, 74.78.−w

I. INTRODUCTION

The research on Fe-based superconductors has been recently boosted by the progress in the techniques of film deposition. Films of very high quality are necessary for applications in superconducting electronics, i.e., for the fabrication of Josephson junctions,[1] superconducting quantum interference devices,[2] and so on. However, they can be fruitfully used also to investigate fundamental properties of these compounds. For instance, they are the perfect playground for transport, optical, and spectroscopic measurements of various kinds; thanks to strain/stress effects that can be induced by the substrate,[3] thin films offer an additional way to tune the critical temperature; finally, they are necessary to realize some proposed phase-sensitive experiments[4] to determine the order parameter symmetry ($s{+}{+}$ or $s\pm$).

So far, thin films of 122 Fe-based compounds have been used to investigate, for example, the gap amplitude and structure, which are probably the most intriguing open issues of these superconductors. As a matter of fact, the emergence of zeros or nodes in the gap has been predicted theoretically within the $s\pm$ symmetry[5–8] as a result of the strong sensitivity of the Fermi surface (FS) to the details of the lattice structure. In 10% Co-doped $BaFe_2As_2$ (Ba-122) thin films, measurements of the complex dynamical conductivity[9] have shown a small isotropic gap of about 3 meV and a larger, highly anisotropic gap of about 8 meV—possibly featuring vertical node lines—located on the electronlike FS sheet. A superconducting gap of 2.8 meV has been measured also by terahertz conductivity spectroscopy in thin films of the same compound with $T_c = 19$ K, but has been associated with the electronlike FS.[10] Optical reflectivity and complex transmittivity measurements in Co-doped Ba-122 films (with nominal $x = 0.10$) have given instead an isotropic gap of 1.85 ± 0.15 meV,[11] but have also shown a low-frequency absorption much stronger than expected for an s-wave gap. Further measurements of optical conductivity and permittivity in similar films allowed discriminating a small gap $\Delta_S = 1.85$ meV on the electronlike FS and a larger gap $\Delta_L = 3.95$ meV on the holelike FS.[12] Recent transmittance and reflectance measurements at terahertz frequencies in ultrathin films with $x = 0.08$ and $T_c = 17.5$ K have given even smaller gaps, i.e., $\Delta_S \simeq 1.0$ meV and $\Delta_L \simeq 2.1$ meV.[13]

Clearly, the results collected up to now do not give a consistent picture, either about the presence and location of the nodal lines, or about the amplitude of the gaps. To try to address this point, we have performed point-contact Andreev-reflection spectroscopy (PCARS) measurements in epitaxial $Ba(Fe_{1-x}Co_x)_2As_2$ thin films with nominal Co content x ranging from 0.04 to 0.15, i.e., from the underdoped to the overdoped region of the phase diagram. The PCARS spectra do not show any clear hint of the emergence of extended node lines, and can be well fitted by the two-band two-dimensional (2D) Blonder-Tinkham-Klapwijk (BTK) model using isotropic gaps—although the shape of the spectra does not allow excluding some degree of gap anisotropy. The dependence of the gap amplitudes Δ_S and Δ_L on the local critical temperature T_c^A is discussed. In underdoped and optimally doped films, the gap ratios are $2\Delta_S/k_B T_c \simeq 3.7$ and $2\Delta_L/k_B T_c \simeq 9$, but decrease to 2.6 and 6.5, respectively, in the overdoped region. When analyzed within a three-band Eliashberg model, these results turn out to be perfectly compatible with $s\pm$ superconductivity mediated by spin fluctuations, whose characteristic energy is $\Omega_0^{sf} = 4.65 k_B T_c$ (as found experimentally by neutron scattering experiments[14]). A reduction of the electron-boson coupling strength is observed in the overdoped regime, which can be rationalized as being related to the suppression of spin fluctuations in this region of the phase diagram.

II. EXPERIMENTAL DETAILS

The $Ba(Fe_{1-x}Co_x)_2As_2$ thin films with a thickness of 50 nm were deposited on (001)CaF_2 substrates by pulsed laser deposition[15] using a polycrystalline target with high phase purity.[15,16] The surface smoothness was confirmed by *in situ* reflection high energy electron diffraction during the deposition; only streaky patterns were observed for all films indicative of smooth surfaces. The details of the structural characterization and of the microstructure of these high-quality, epitaxial thin films can be found in Ref. 15. Standard four-probe resistance measurements were performed in a ^{4}He cryostat to determine the transport critical temperature and the transition widths, reported in Table I. With respect to most phase diagrams of $Ba(Fe_{1-x}Co_x)_2As_2$ single crystals,[17–19] where the optimal doping corresponds to $x \simeq 0.065$, the highest T_c^{90} of our films (i.e., the temperature at which the resistance is 90% of its normal-state value immediately before the transition) is attained for $x = 0.10$, and in the $x = 0.15$ sample T_c^{90} is still about 22 K. This wide doping range of high T_c is presumably due to a combination of epitaxial strain from the substrate and of reduced Co content in the film with respect to the nominal one. Detailed investigation is under way. In the following of this paper we will therefore always refer to the doping content of the target. This does not hamper our discussion, since we will refer all the results to the critical temperature of the contact, which is a local property directly correlated to the gap amplitudes (as we have already demonstrated in many different cases[20]) and is thus well defined irrespectively of the actual Co content.[21]

PCARS measurements have been performed by using the "soft" technique we introduced many years ago,[22] in which a thin Au wire ($\varnothing = 18\ \mu$m) is kept in contact with the film surface by means of a small drop ($\varnothing \leqslant 100\ \mu$m) of Ag conducting paste. The effective size of the point contact (PC) is of course much smaller than the area covered by the Ag paste: Parallel nanoscopic contacts are likely to be formed here and there, between individual Ag grains and the sample surface. This technique has some advantages over the conventional "needle-anvil" one and has indeed been adopted also by other groups.[23,24] In the specific case of the Co-doped Ba-122 films we studied here, conventional point-contact measurements gave either featureless spectra, or spectra far from ideality, with a small Andreev signal superimposed to a background strongly decreasing with bias voltage,[25] while the soft technique provides very often good spectra with a clear spectroscopic signal, as we will show in the following. Analyses of the surface of these films carried out by means of atomic force microscopy, x-ray photoemission spectroscopy, and scanning spreading resistance microscopy[25] have provided an explanation for this difference. They have shown the presence of a thin, inhomogeneous, poorly conducting layer, due to reaction with air, that makes the local conductivity of the surface highly position dependent. In these conditions, since the conventional technique probes a very small portion of the surface, the probability of making the contact in a clean region is rather low. In contrast, the drop of Ag paste used in the soft technique covers a larger surface and allows a natural selection of the more conducting channels within a micrometric region.

TABLE I. Critical temperatures of our films determined from electric transport measurements. T_c^{90} and T_c^{10} are the temperatures at which the resistance (the resistivity) is 90% and 10% of the normal-state value immediately before the transition. ΔT_c is defined here as $(T_c^{90} - T_c^{10})$.

x	T_c^{90} (K)	T_c^{10} (K)	ΔT_c (K)
0.04	9.5	7.0	2.5
0.08	25.6	24.2	1.4
0.08	25.4	23.9	1.5
0.08	25.4	23.6	1.8
0.10	26.6	24.6	2.0
0.15	22.0	20.6	1.4

The PCARS spectra simply consist of the differential conductance dI/dV of the N-S contact, as a function of the voltage. In principle, a point contact can provide spectroscopic information only if the conduction is ballistic, i.e., electrons do not scatter in the contact region. This is achieved if the contact radius a is smaller than the electronic mean free path, ℓ.[26] According to Sharvin's[27] or Wexler's[28] equations, a is also related to the normal-state contact resistance R_N. The fact that in these films most of the contacts, irrespective of their resistance, do show clear Andreev signals is again related to the particular nature of the film surface and to the fact that each contact is actually the parallel of many nanoscopic contacts. As a matter of fact, the high residual resistivity (120 $\mu\Omega$ cm for $x = 0.10$) of the films implies a small mean free path ℓ, reasonably of the order of a few nanometers (even though its precise determination from the resistivity is not straightforward and would at least require the calculation of the plasma frequencies of the different bands). In these conditions [analogous to those discussed in the case of PCARS on thin films of SmFeAs(O,F) and LaFeAs(O,F)[29]] the ballistic—or, at least, the diffusive[26]—regime can only be achieved when the (microscopic) PC is the parallel of several nanoscopic contacts that fulfill the ballistic or diffusive conditions, and whose individual resistance is thus much greater than that of the microscopic contact as a whole. This occurs rather naturally in our films thanks to the surface characteristics mentioned above.

Owing to the epitaxial structure of the films and to the smoothness of their surface, the current that flows through the point contact is mainly parallel to the crystallographic c axis. By placing the contacts in different regions of the sample surface, we were able to check the homogeneity of the superconducting properties and to obtain some information about their distribution. To allow a comparison of the experimental dI/dV vs V curves to the theoretical models, the former must be first normalized, i.e., divided by the normal-state conductance curve $(dI/dV)_N$ vs V (in principle, recorded at the same temperature). This curve is inaccessible to experiments because of the very high upper critical field, and the normal-state conductance measured just above T_c is unusable because of an anomalous shift of the conductance curves across the superconducting transition, clearly visible in Fig. 1. This effect is typical of very thin films and is related to a temperature- and current-dependent spreading resistance contribution arising from the portion of the film between the point contact and the second voltage electrode.[30] A quantitative

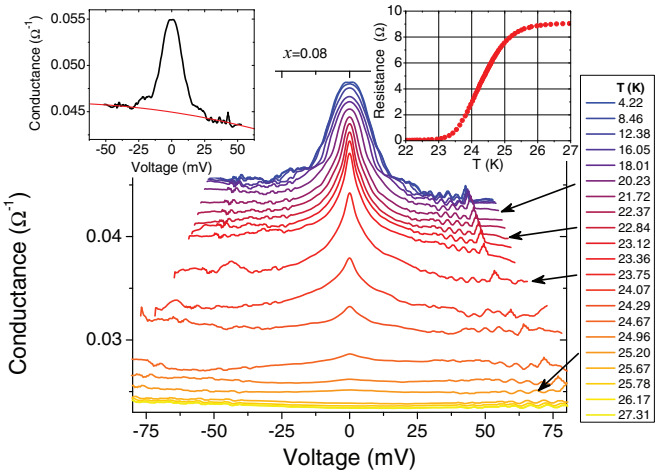

FIG. 1. (Color online) Temperature dependence of the spectrum of a point contact on an 8% Co-doped film, up to the critical temperature and above. The shift of the spectra is clearly seen. The left inset shows the low-temperature spectrum and the polynomial curve that fits its tails used for normalization. The right inset reports the temperature dependence of the resistance of the film. The shift of the spectra correlates with the onset of resistivity in the film. Here, T_c^A is between 25.20 and 25.67 K, i.e., $T_c^A \simeq 25.4 \pm 0.3$.

model has been recently proposed in Ref. 31. For these reasons, as shown in detail elsewhere,[32] the normalization can be rather critical in Fe-based compounds; here we chose to divide the low-temperature conductance curves by a polynomial fit of their own high-voltage tails, as shown in the left inset of Fig. 1. For the same reason, we will here concentrate on the low-temperature spectra.

The normalized curves were fitted with the BTK model generalized by Kashiwaya and Tanaka[33,34] (later on called the "2D-BTK model") in order to extract the gap values, as discussed in the following section. This model is based on the assumption of spherical FSs in both the normal metal and the superconductor, which is clearly a strong simplification in the case of Fe-based compounds. A more refined (and complicated) three-dimensional-BTK model[32,35] could be used to calculate the conductance curves accounting for the real shape of the FS but, as shown elsewhere,[36,37] this would not significantly change the resulting gap amplitudes. The local critical temperature (in the following indicated by T_c^A) can be determined by simply looking at the temperature dependence of the raw conductance curves; T_c^A is identified with the temperature at which the features related to Andreev reflection disappear, and its uncertainty is determined by the width of the temperature steps between the acquired spectra. The T_c^A values were generally in very good agreement with the critical temperature of the whole film determined by resistance measurements and/or susceptibility or magnetization measurements since in most cases they fall between T_c^{10} and T_c^{90}. A noticeable exception is the underdoped sample ($x = 0.04$) in which some spectra show a zero-bias peak that becomes clearer on increasing temperature and persists in the normal state. This effect has also been observed by other groups[24,38,39] and might be related to some magnetic scattering rather than to superconductivity. This issue is still under debate[24] and will be addressed in a forthcoming paper. Here, however, we will only report PCARS spectra that do not show this anomaly.

III. RESULTS AND DISCUSSION

Figure 2 shows some representative examples of the many PCARS spectra recorded in films at different doping (symbols), from $x = 0.04$ (top panel) to $x = 0.15$ (bottom panel). For $x \geqslant 0.08$ the shape of all the curves is clearly incompatible with a single gap. These spectra show two symmetric maxima at low energy (or a small flat region around zero bias, as in the bottom panel) which are the hallmark of the small gap Δ_S, plus additional shoulders or changes in slope at higher energy that are due to the second, larger gap Δ_L. The case of $x = 0.04$, where the double-gap structure is not evident, is in some sense anomalous and will be discussed in more detail later. The additional structures often visible at higher energy (about 20 meV for $x \geqslant 0.08$) are related to the strong coupling between electrons and spin fluctuations, as shown in detail elsewhere.[32,40] Here, we are mainly interested in the gap amplitudes, and we will thus disregard these structures (note

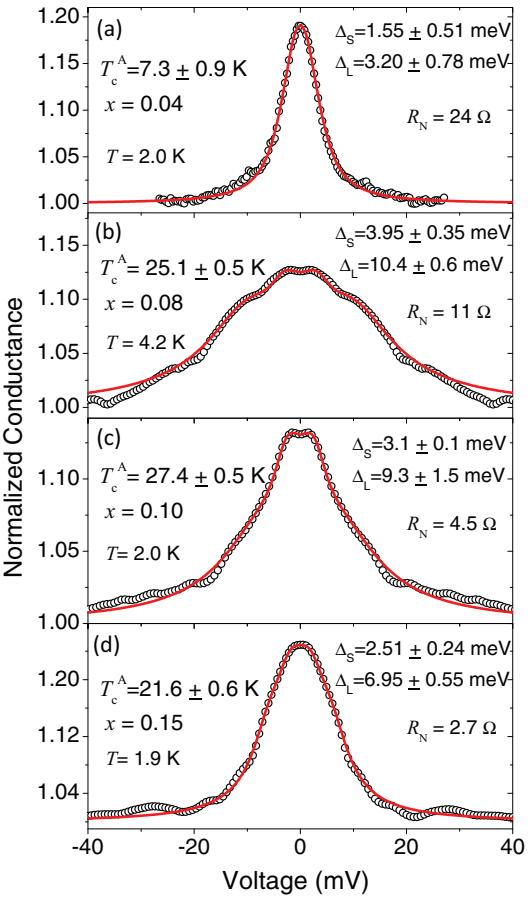

FIG. 2. (Color online) Low-temperature normalized PCARS spectra (symbols) in films with different Co content: $x = 0.04$ (a), $x = 0.08$ (b), $x = 0.10$ (c), and $x = 0.15$ (d), together with their two-band 2D-BTK fit (lines). The corresponding fitting parameters are listed in Table II. The gap values Δ_S and Δ_L indicated in the panels are instead the average over different possible fits of the same curve, as explained in the text. The normal-state resistance of the contacts is also indicated, as well as the local critical temperature T_c^A.

TABLE II. Fitting parameters of the spectra shown in Fig. 2. Each set of parameters is relevant to the individual BTK curve shown in the corresponding panel of Fig. 2. The gaps Δ_S and Δ_L and the broadening parameters Γ_S and Γ_L are expressed in meV. The uncertainty on the gap ratio is due to the uncertainty on the critical temperature (see Fig. 2).

x	Δ_S	Γ_S	Z_S	Δ_L	Γ_L	Z_L	w_S	$2\Delta_S/k_BT_c^A$	$2\Delta_L/k_BT_c^A$
0.04	1.80	1.52	0.16	3.60	2.59	0.17	0.48	5.73 ± 0.71	11.47 ± 1.41
0.08	3.90	2.70	0.23	10.60	7.00	0.39	0.40	3.61 ± 0.07	9.82 ± 0.20
0.10	3.20	2.40	0.25	8.80	7.30	0.32	0.50	2.72 ± 0.05	7.47 ± 0.14
0.15	2.75	2.03	0.20	7.00	2.90	0.20	0.50	2.96 ± 0.08	7.54 ± 0.21

that their presence does not affect in any way the values of the gaps extracted from the fit, as shown in Refs. 40 and 32).

Solid lines superimposed to the experimental data of Fig. 2 represent their best fit within the two-band 2D-BTK model. This model assumes that the total conductance is simply the sum of the partial contributions from two sets of equivalent bands, i.e., holelike and electronlike, and each contribution can be calculated by using the 2D-BTK model. The model thus contains seven adjustable parameters: the two gap amplitudes Δ_S and Δ_L, the broadening parameters Γ_S and Γ_L, the barrier parameters Z_S and Z_L, and the relative weight of the two bands that contribute to the conductance (w_S and $w_L = 1 - w_S$).[41] The values of these parameters for the curves shown in Fig. 2 are reported in Table II. Because of the number of parameters, the set of their best-fitting values for a given spectrum is not univocal, especially when the signal is not very high as in Fe-based compounds. To account for this, we always determined the maximum possible range of Δ_S and Δ_L values compatible with a given curve, when all the other parameters are changed as well. Based on the results obtained in $Ba(Fe_{1-x}Co_x)_2As_2$ single crystals at optimal doping,[40] we initially assumed the two gaps to be isotropic. This assumption works well in the *whole* doping range analyzed here, thus indicating that there are no clear signs of a change in the gap symmetry and structure on increasing the doping content. In this respect it should be noted that the 2D-BTK model is not the most sensitive to the subtle details of the gap structure, so this result does not exclude gap anisotropies either in the plane or in the c direction whose existence has been claimed or predicted in Co-doped Ba-122 (Ref. 42) and more generally in the 122 systems.[6,8] It must be noted, however, that if extended node lines (predicted in particular conditions in 122 compounds[7]) were present, they would give rise to quasiparticle excitations with very small energy that *can* be detected by PCARS, as shown in the case of $Ca(Fe,Co)_2As_2$.[43]

Figure 3 shows two examples of the many (almost 20) conductance curves measured in three different films with $x = 0.08$. The curves have different shapes but the values of the gaps extracted from their fit (indicated in the legend) are compatible with one another. The other fitting parameters are listed in the caption. As shown in panel (c) of the same figure, there is no correlation between the gap values extracted from the fit of different spectra and the resistance of the contact. This fact supports the spectroscopic nature of the contacts[26] and excludes the presence of spreading-resistance effects[30] in our measurements at low temperature. More generally, the consistency of the gap values obtained in different regions of the *same* film is good proof of the macroscopic homogeneity of the superconducting properties, while the consistency of the values obtained in *different* films with the same doping is proof of the reproducibility of the deposition process.

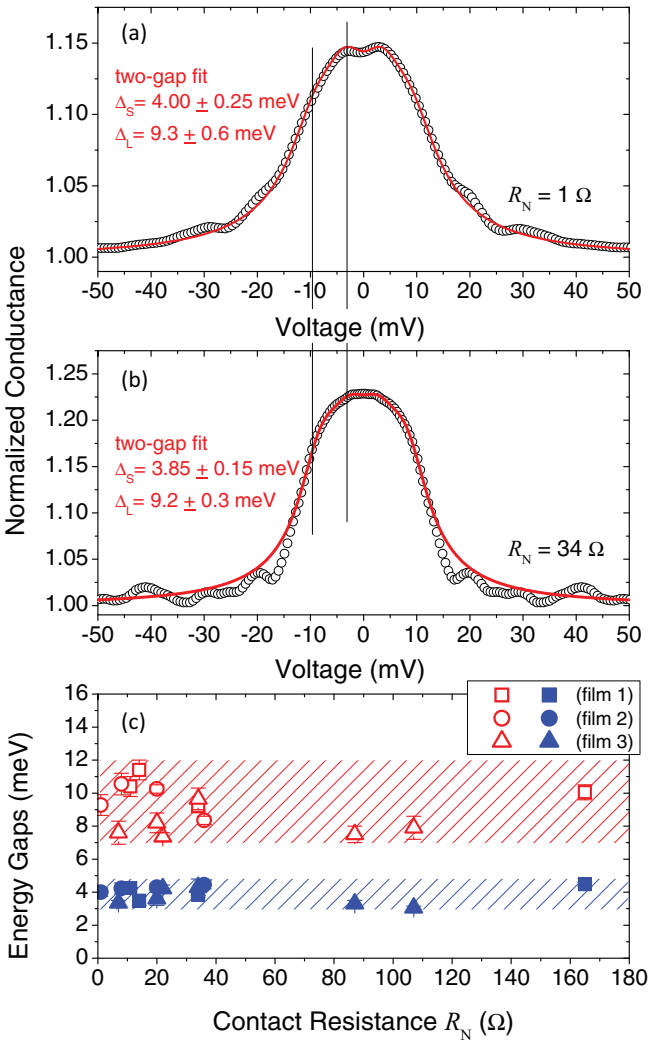

FIG. 3. (Color online) (a), (b) Two examples of PCARS spectra taken in different films of $Ba(Fe_{0.92}Co_{0.08})_2As_2$. Despite the different shape of the spectra, the gap values obtained from the fit are consistent. The fit shown in (a) was obtained with $\Delta_S = 4.25$ meV, $\Gamma_S = 3.60$ meV, $Z_S = 0.25$, $\Delta_L = 9.90$ meV, $\Gamma_L = 4.70$ meV, $Z_L = 0.34$, $w_L = 0.60$. The fit in (b) was obtained with $\Delta_S = 3.70$ meV, $\Gamma_S = 2.35$ meV, $Z_S = 0.18$, $\Delta_L = 9.00$ meV, $\Gamma_L = 3.25$ meV, $Z_L = 0.30$, $w_L = 0.40$. (c) Gap amplitudes as a function of the resistance of the contacts, which shows the absence of any correlation between these quantities and demonstrates the spectroscopic nature of the contacts. This panel includes data taken in three different films.

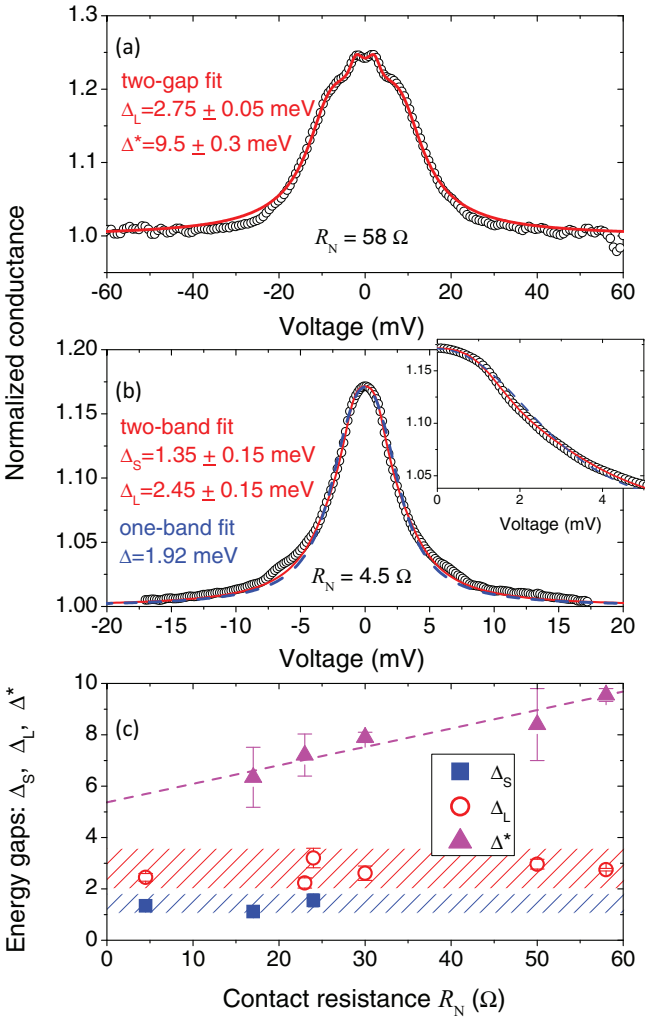

FIG. 4. (Color online) (a), (b) Two examples of PCARS spectra taken in different points of the same film ($5 \times 5\,\mathrm{mm}^2$) of $Ba(Fe_{0.96}Co_{0.04})_2As_2$. The spectrum in (a) shows clear shoulders around 7 meV and conductance maxima at lower energy. The solid line represents the best fit of the curve obtained within the 2D-BTK model assuming that the shoulders are due to a superconducting gap Δ^*. The fitting parameters are $\Delta_L = 2.8$ meV, $\Gamma_L = 1.15$ meV, $Z_L = 0.24$, $\Delta^* = 9.8$ meV, $\Gamma^* = 4.75$ meV, $Z^* = 0.25$, $w_S = 0.2$. The spectrum in (b) instead does not show shoulders but a single maximum at zero bias, and the FWHM of the whole structure is of the order of 3 meV. The solid line is the two-band BTK fit, obtained with parameters $\Delta_S = 1.35$ meV, $\Gamma_S = 0.84$ meV, $Z_S = 0.18$, $\Delta_L = 2.6$ meV, $\Gamma_L = 1.8$ meV, $Z_L = 0.4$, $w_S = 0.6$. The dashed line is the single-band BTK fit, obtained with parameters $\Delta = 1.92$ meV, $\Gamma = 1.74$ meV, $Z = 0.12$. A magnification of the low-energy region (inset) shows that the two-gap fit is better. (c) Amplitudes of the "gap" Δ^* and of the gaps Δ_S and Δ_L as a function of the contact resistance R_N.

For $x = 0.04$ the spectra often show very clear shoulders at energies of the order of 7 meV in addition to conductance maxima at about 3 meV, as shown in Fig. 4(a). The shoulders are fast suppressed on increasing temperature or upon application of a magnetic field (they look completely washed out already at 5 K, or in a field of 1 T). If one assumes that they are due to a superconducting gap and fits the spectra with the two-band 2D-BTK model, the relevant amplitude Δ^* turns out to be of the order of 6–9 meV. Since the measured film showed a T_c^{90} of less than 10 K, these values are clearly unphysical for a superconducting gap. The smaller gap obtained from the same 2D-BTK fit turns out to range between 1.1 and 3.2 meV and its Andreev signal shows a conventional dependence on temperature and magnetic field. In a small number of spectra, of which an example is shown in Fig. 4(b), the structures at about 7 meV are not present at all and a single, much narrower structure is observed, whose width is of the order of 3 meV. These spectra admit a fit with the single-gap BTK model, giving a gap of the order of 2 meV, but the two-band BTK model still works better [see the inset to Fig. 4(b)] and gives a small gap Δ_S of the order of 1.5 meV and a larger gap Δ_L of about 2.5–3.0 meV. Although this fact alone does not allow concluding that in this compound two gaps survive, we will refer from now on to the results of the two-gap fit on the basis of plausibility arguments. Indeed, even at 4% Co doping, the Ba-122 system retains a multiband electronic structure and there is no reason to believe that the two gaps observed at higher doping should "merge" into one. This effect is theoretically predicted in the presence of strong disorder[44] but would be accompanied by a strong suppression of the critical temperature, while the T_c of our 4% Co-doped film is identical to that of single crystals with the same Co content, where two gaps have been measured by specific heat.[45]

Figure 4(c) shows a summary of the values of Δ_S, Δ_L, and Δ^* obtained from the two-band fit of spectra of the first and second type, plotted as a function of the resistance of the contacts R_N. Clearly, the larger "energy scale" Δ^* depends on the contact resistance, which (together with the anomalous dependence on temperature and magnetic field) indicates that the structures around 7 meV are not due to a superconducting gap. Further confirmation comes from the weight of Δ^* in the fit, which depends on R_N (unlike for superconducting gaps), decreasing from 0.8 to 0.6 when R_N goes from 58 Ω to 17 Ω. This reflects the fact that the amplitude of the relevant structures decreases on decreasing R_N; consequently, their position is less easily identifiable (which may partly account for the dependence of Δ^* from R_N). On this basis, understanding the origin of these structures is a difficult task. The 4% doped sample falls well in the region of the phase diagram where superconductivity and magnetism coexist, and which is still poorly understood. One might speculate that these structures arise from a magnetic phase probed by a subset of nanocontacts; the amplitude of the relevant signal in the spectrum, as well as the resistance of the contact as a whole, may thus be related to the fraction of conduction channels in this phase.

Going back to Fig. 4(c), the smaller gaps do not show any dependence on the contact resistance and seem to cluster in two groups indicated by squares and circles for clarity. Although the two energy ranges are very close to each other, they do not overlap (even taking into account the error bars), further supporting the picture of *two* gaps Δ_S and Δ_L.

Figure 5 reports the (average) gap amplitudes Δ_S and Δ_L obtained in the various films as a function of the (average) T_c^A of the contacts. In other words, the values of Δ_S and Δ_L reported here are the midpoints of the corresponding range of gap amplitudes obtained in the fit of different curves. The width

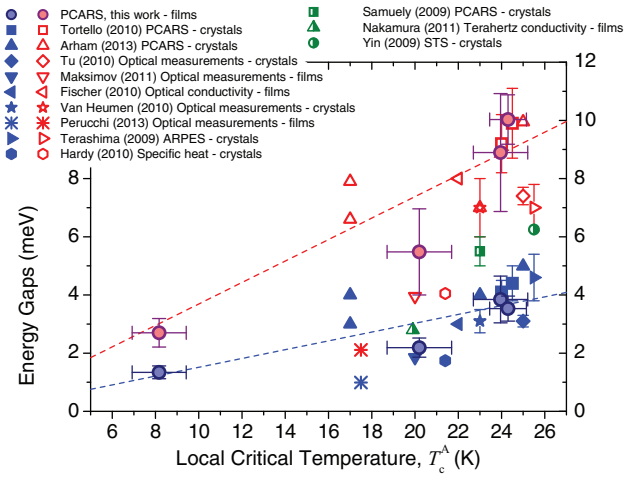

FIG. 5. (Color online) Average gap amplitudes in $Ba(Fe_{1-x}Co_x)_2As_2$ thin films with different Co content obtained by PCARS measurements (filled circles), plotted as a function of T_c^A. The other data points are taken from literature, and specifically squares from Ref. 40, up triangles from Ref. 24, diamonds from Ref. 47, down triangles from Ref. 12, left triangles from Ref. 9, stars from Ref. 65, asterisks from Ref. 13, right triangles from Ref. 49, hexagons from Ref. 48, half-filled squares from Ref. 46, half-filled circles from Ref. 10, and half-filled triangles from Ref. 50. The techniques used for these measurements are indicated in the legend. The upper and lower dashed lines correspond to a gap ratio $2\Delta/k_BT_c$ equal to 3.52 and 9.0, respectively.

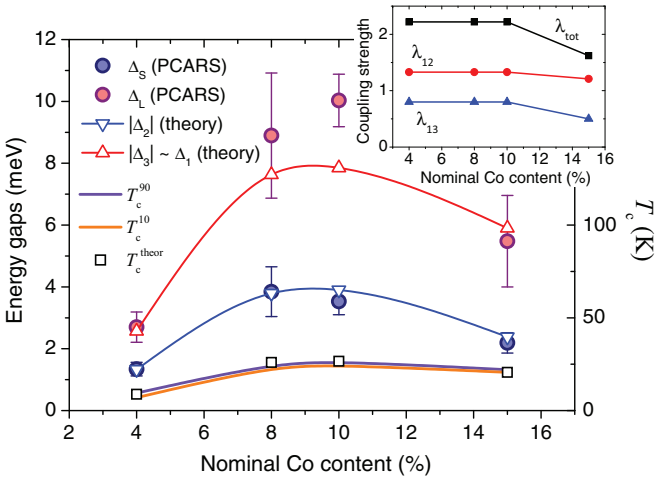

FIG. 6. (Color online) Doping dependence of the gaps measured by PCARS (circles, left vertical scale) and of the critical temperature from resistivity measurements (lines, right vertical scale). Triangles and squares indicate the values of the gaps and of the critical temperature calculated within the three-band Eliashberg model described in the text. The inset shows the dependence of the coupling strengths λ_{12} and λ_{13} on the Co content, together with the total electron-boson coupling constant.

of the range is represented by the vertical error bars, while the horizontal error bars indicate the range of T_c^A values in all the point contacts made on that film. Figure 5 also shows the results of PCARS in single crystals[24,40,46] as well as the gap amplitudes determined either in films or single crystals by means of other techniques, namely, optical measurements,[9,10,12,47] specific heat,[48] angle-resolved photoemission spectroscopy (ARPES)[49] and scanning tunneling spectroscopy.[50]

At the highest T_c values, corresponding to $x = 0.08$ and $x = 0.10$, the gap values agree rather well with those given by PCARS in single crystals.[24,40] The large spread of Δ_L values given by PCARS has already been noticed in various Fe-based compounds[32] and its origin may be either intrinsic (e.g., anisotropy of Δ_L) or extrinsic (uncertainty due to the normalization). Finally, the values given by PCARS (especially for Δ_L) are systematically larger than those given by optical measurements and specific-heat measurements. This may be due to the approximations on which the fit of the curves is based, but may also hide some more fundamental property of Fe-based compounds. The small gap Δ_S appears much better defined; the values provided by different techniques are well consistent with one another. Concerning the gap values away from optimal doping, it should be borne in mind that Fig. 5 reports in the same plot the data for underdoped and overdoped samples; in particular, the points at $T_c = 20.2$ K refer to the $x = 0.15$ film. If these points are temporarily excluded from the analysis, a roughly linear trend of the gaps as a function of T_c can be observed. The dashed lines in Fig. 5 have equations $2\Delta/k_BT_c = 3.52$ and $2\Delta/k_BT_c = 9.0$; it can be clearly seen that the small gap is approximately BCS for any x between 0.04 and 0.10. Even though Δ_L is affected by a much larger uncertainty, it can be said that $2\Delta_L/k_BT_c$ ranges between 7 and 10 in the same doping range. The points at $x = 0.15$ are instead outside this trend since the gap values here correspond to reduced gap ratios. This point can be clarified by plotting the gap amplitudes as a function of the nominal doping, as in Fig. 6.

As expected, the trend of the gaps mimics the trend of the critical temperature, showing a maximum at $x = 0.08$–0.10. However, the trend is not symmetric in the sense that in the overdoped region the gaps decrease "more" than the critical temperature, i.e., the gap ratios decrease. The theoretical analysis of these results is presented in the following section.

IV. INTERPRETATION OF THE RESULTS WITHIN ELIASHBERG THEORY

We have shown elsewhere[51,52] that a simple three-band Eliashberg model with a very small number of free parameters can account surprisingly well for the phenomenology of Fe-based superconductors and allows explaining a large variety of their properties. Here we use the same model to try to rationalize the experimental trend of the gaps as a function of T_c or of the doping content x. The first assumption of the model is that the electronic structure of $Ba(Fe_{1-x}Co_x)_2As_2$ can be approximately described by one hole band (indicated in the following as band 1) and two electron bands (2 and 3).[40,52] The gap symmetry is assumed to be $s\pm$ (Ref. 53) so that the sign of Δ_1 (here assumed positive) is opposite to that of Δ_2 and Δ_3. Although PCARS, as well as many other spectroscopic techniques, provides at most two gap amplitudes and does not allow associating them to a particular FS sheet, the use of (at least) three effective bands and thus three gaps is necessary for the Eliashberg model to be able to reproduce the experimental results. However, ARPES results

in optimally Co-doped Ba-122 single crystals indicated that the larger gap belongs to the holelike FS sheet.[49] With this in mind, we will assume $\Delta_1 \simeq |\Delta_3|$ and $|\Delta_2|$ to be the large and the small gaps measured by PCARS, respectively. This assumption is consistent with the fact that the experimental results do not resolve the two larger gaps. To obtain the gaps and the critical temperature within the s± wave three-band Eliashberg model[54] one has to solve six coupled equations for the gaps $\Delta_i(i\omega_n)$ and the renormalization functions $Z_i(i\omega_n)$, where i is a band index ($i = 1.3$). The equations have been reported elsewhere;[51] their solution requires a large number of input parameters (18 functions and 9 constants); however, some of these parameters are correlated, some can be extracted from experiments, and some can be fixed by suitable approximations. For example, the coupling constant matrix λ_{ij} can be greatly simplified. In general, one should consider that each matrix element has one contribution from phonons and one from antiferromagnetic (AFM) spin fluctuations (SF), i.e. $\lambda_{ij} = \lambda_{ij}^{ph} + \lambda_{ij}^{sf}$. However, the coupling between the two electron bands is small, and we thus take $\lambda_{23} = \lambda_{32} = 0$; the total electron-phonon coupling in pnictides is generally small[55] and phonons mainly provide intraband coupling, so that we assume $\lambda_{ij}^{ph} = 0$; spin fluctuations mainly provide interband coupling between the two quasi-nested FS sheets,[53] and thus we assume $\lambda_{ii}^{sf} = 0$. Finally, the electron-boson coupling-constant matrix λ_{ij} takes the following form:[40,51,56]

$$\lambda_{ij} = \begin{pmatrix} \lambda_{11}^{ph} & \lambda_{12}^{sf} & \lambda_{13}^{sf} \\ \lambda_{21}^{sf} & \lambda_{22}^{ph} & 0 \\ \lambda_{31}^{sf} & 0 & \lambda_{33}^{ph} \end{pmatrix}, \quad (1)$$

where $\lambda_{21}^{sf} = \lambda_{12}^{sf}\nu_{12}$ and $\lambda_{31}^{sf} = \lambda_{13}^{sf}\nu_{13}$, with $\nu_{ij} = N_i(0)/N_j(0)$ and $N_i(0)$ is the normal density of states at the Fermi level for the ith band. Another fundamental ingredient is the electron-boson spectral function $\alpha^2F(\Omega)$ of the boson responsible for the pairing. The shape of the electron-phonon spectral function is taken from literature[57] and we assume $\alpha_{11}^2F^{ph}(\Omega) = \alpha_{22}^2F^{ph}(\Omega) = \alpha_{33}^2F^{ph}(\Omega)$ with $\lambda_{ii}^{ph} = 0.2$.[58] As for spin fluctuations, we assume their spectrum to have a Lorentzian shape:[51,59–61]

$$\alpha_{ij}^2F^{sf}(\Omega) = C_{ij}\{L(\Omega + \Omega_{ij}, Y_{ij}) - L(\Omega - \Omega_{ij}, Y_{ij})\}, \quad (2)$$

where $L(\Omega \pm \Omega_{ij}, Y_{ij}) = \frac{1}{(\Omega \pm \Omega_{ij})^2 + Y_{ij}^2}$. C_{ij} are normalization constants, necessary to obtain the proper values of λ_{ij} while Ω_{ij} and Y_{ij} are the peak energies and half-widths of the Lorentzian functions, respectively.[51] In all the calculations we set $\Omega_{ij} = \Omega_0^{sf}$ and $Y_{ij} = Y_{ij}^{sf} = \Omega_0^{sf}/2$.[14] Here, Ω_0^{sf} is the characteristic energy of the AFM SF, assumed to be equal to the spin-resonance energy, as verified experimentally by us in optimally Co-doped Ba-122 single crystals.[32,40] Its value is determined according to the empirical relation $\Omega_0^{sf} = 4.65k_BT_c$ (proposed in Ref. 62). Band-structure calculations provide information about the factors ν_{ij} that enter the definition of λ_{ij}. In the case of optimally doped $Ba(Fe_{1-x}Co_x)_2As_2$, $\nu_{12} = 1.12$ and $\nu_{13} = 4.50$.[63] As a first approximation, these values have been used here for all Co contents. Moreover, based on the fact that the Coulomb pseudopotential is probably small in these compounds[8] we assume all the elements of the pseudopotential matrix to be identically zero ($\mu_{ii}^* = \mu_{ij}^* = 0$); finally, we neglect the effect of disorder, owing to the high quality of the films.

Finally, only two free parameters remain, i.e., the coupling constants λ_{12}^{sf} and λ_{13}^{sf}. These parameters can be tuned in such a way to reproduce the experimental values of the small gap Δ_S and of the critical temperature, which are the best-defined experimental data; the values of the large gap Δ_L are indeed affected by a larger relative uncertainty, and moreover they might actually be a sort of weighted "average" of the two gaps Δ_1 and $|\Delta_3|$. The larger gaps are therefore calculated with the values of λ_{12}^{sf} and λ_{13}^{sf} that allow reproducing Δ_S and T_c.

The result of these calculations is that (i) the trend of the experimental gaps Δ_S and Δ_L as a function of T_c and of x in the samples with nominal Co content $x = 0.04$, 0.08, and 0.10 can be reproduced by using $\lambda_{12}^{sf} = 0.8$ and $\lambda_{13}^{sf} = 1.33$, and only changing the value of the characteristic SF energy Ω_0 according to the change in T_c; (ii) to reproduce the values of the gaps and of T_c in the overdoped sample ($x = 0.15$) it is instead also necessary to reduce the values of the two coupling constants: $\lambda_{12}^{sf} = 0.5$ and $\lambda_{13}^{sf} = 1.21$. The values of these two parameters are shown as a function of x in the inset of Fig. 6. Note that the total coupling is $\lambda_{tot} = 2.22$ for $x = 0.04$, 0.08, and 0.10 and decreases to $\lambda_{tot} = 1.82$ at $x = 0.15$. These values are in agreement with those found in previous works,[52,58] and indicate that Co-doped Ba-122 is a strong-coupling superconductor at all the doping contents analyzed here. The main panel of Fig. 6 also reports the calculated values of the gaps as a function of x. The agreement between the theoretical and experimental values of T_c and of the small gap is very good; the large gap is underestimated around optimal doping, but the trend is qualitatively correct. The agreement might be improved if the feedback effect of the condensate on the bosonic excitations[60,61] was taken into account, which was not done in this paper for simplicity.

V. CONCLUSIONS

In conclusion, we have determined the energy gaps of $Ba(Fe_{1-x}Co_x)_2As_2$ in a wide range of nominal doping ($0.04 \leqslant x \leqslant 0.15$) by means of soft PCARS measurements in epitaxial thin films. Several PCARS spectra were acquired on each sample, with the probe current injected perpendicular to the film surface and thus mainly along the c axis. For any $x \geqslant 0.08$ the PCARS spectra admit a fit with the two-band 2D-BTK model using two isotropic gaps, and their shape does not suggest the presence of node lines on the FS; in the strongly underdoped sample ($x = 0.04$) a fit with a single isotropic gap is also possible, though a little worse than the two-gap one. Altogether, these results show no clear hints of changes in the gap symmetry or structure in the doping range of our films—although the shape of the spectra does not allow excluding some degree of gap anisotropy.

The small gap turns out to be approximately BCS, with a ratio $2\Delta_S/k_BT_c = 3.7 \pm 0.8$ (the uncertainty arises from the statistical spread of gap values) for $x \leqslant 0.10$, and smaller (2.6 ± 0.3) at $x = 0.15$. The second gap is much larger, with a ratio $2\Delta_L/k_BT_c$ of the order of 9 for $x \leqslant 0.10$ and 6.5 for $x = 0.15$.

The trend of the gaps and of T_c as a function of the Co content can be reproduced by a simple $s\pm$ Eliashberg model in which the spectrum of the mediating boson is that of spin fluctuations, and its characteristic energy coincides with the energy of the spin resonance. The decrease of the gap ratios in the overdoped samples is reflected in the values of the coupling strengths that are constant for $x \leqslant 0.10$ and slightly decrease at $x = 0.15$. This result finds a natural explanation within the picture of $s\pm$ superconductivity mediated by spin fluctuations: In the overdoped regime, far from the AFM region of the phase diagram, superconductivity may suffer from a suppression of the spin fluctuations and the loss of nesting,[64] which could lead to a decrease in the superconducting interband coupling that, in turn, produces a larger decrease of the gaps in comparison with the reduction of the critical temperature.

ACKNOWLEDGMENTS

D.D. and P.P. wish to thank the Leibniz Institute for Solid State and Materials Research (IFW) in Dresden, Germany, and in particular, the Department of Superconducting Materials, where many of the PCARS measurements were performed. Particular thanks to V. Grinenko, J. Hänisch, and K. Nenkov for valuable discussions and technical support. This work was done under the Collaborative EU-Japan Project "IRON SEA" (NMP3-SL-2011-283141).

[1] P. Seidel, Supercond. Sci. Technol. **24**, 043001 (2011).
[2] T. Katase, Y. Ishimaru, A. Tsukamoto, H. Hiramatsu, T. Kamiya, K. Tanabe, and H. Hosono, Supercond. Sci. Technol. **23**, 082001 (2010).
[3] K. Iida, J. Hänisch, R. Hühne, F. Kurth, M. Kidszun, S. Haindl, J. Werner, L. Schultz, and B. Holzapfel, Appl. Phys. Lett. **95**, 192501 (2009).
[4] A. A. Golubov and I. I. Mazin, Appl. Phys. Lett. **102**, 032601 (2013).
[5] K. Kuroki, H. Usui, S. Onari, R. Arita, and H. Aoki, Phys. Rev. B **79**, 224511 (2009).
[6] S. Graser, A. F. Kemper, T. A. Maier, H.-P. Cheng, P. J. Hirschfeld, and D. J. Scalapino, Phys. Rev. B **81**, 214503 (2010).
[7] K. Suzuki, H. Usui, and K. Kuroki, J. Phys. Soc. Jpn. **80**, 013710 (2011).
[8] P. J. Hirschfeld, M. M. Korshunov, and I. I. Mazin, Rep. Prog. Phys. **74**, 124508 (2011).
[9] T. Fischer, A. V. Pronin, J. Wosnitza, K. Iida, F. Kurth, S. Haindl, L. Schultz, B. Holzapfel, and E. Schachinger, Phys. Rev. B **82**, 224507 (2010).
[10] D. Nakamura, Y. Imai, A. Maeda, T. Katase, H. Hiramatsu, and H. Hosono, Physica C **471**, 634 (2011).
[11] B. Gorshunov, D. Wu, A. A. Voronkov, P. Kallina, K. Iida, S. Haindl, F. Kurth, L. Schultz, B. Holzapfel, and M. Dressel, Phys. Rev. B **81**, 060509 (2010).
[12] E. G. Maksimov, A. E. Karakozov, B. P. Gorshunov, A. Prokhorov, A. A. Voronkov, E. S. Zhukova, V. S. Nozdrin, S. S. Zhukov, D. Wu, M. Dressel *et al.*, Phys. Rev. B **83**, 140502(R) (2011).
[13] A. Perucchi, L. Baldassarre, B. Joseph, S. Lupi, S. Lee, C. B. Eom, J. Jiang, J. D. Weiss, E. E. Hellstrom, and P. Dore, Eur. Phys. J. B **86**, 274 (2013).
[14] D. S. Inosov, J. T. Park, P. Bourges, D. L. Sun, Y. Sidis, A. Schneidewind, K. Hradil, D. Haug, C. T. Lin, B. Keimer *et al.*, Nat. Phys. **6**, 178 (2010).
[15] F. Kurth, E. Reich, J. Hänisch, A. Ichinose, I. Tsukada, R. Hühne, S. Trommler, J. Engelmann, L. Schultz, B. Holzapfel *et al.*, Appl. Phys. Lett. **102**, 142601 (2013).
[16] F. Kurth, K. Iida, S. Trommler, J. Hänisch, K. Nenkov, J. Engelmann, S. Oswald, J. Werner, L. Schultz, B. Holzapfel *et al.*, Supercond. Sci. Technol. **26**, 025014 (2013).
[17] N. Ni, M. E. Tillman, J. Q. Yan, A. Kracher, S. T. Hannahs, S. L. Budko, and P. C. Canfield, Phys. Rev. B **78**, 214515 (2008).
[18] J.-H. Chu, J. G. Analytis, C. Kucharczyk, and I. R. Fisher, Phys. Rev. B **79**, 014506 (2009).
[19] F. L. Ning, K. Ahilan, T. Imai, A. S. Sefat, M. A. McGuire, B. C. Sales, D. Mandrus, P. Cheng, B. Shen, and H.-H. Wen, Phys. Rev. Lett. **104**, 037001 (2010).
[20] D. Daghero and R. Gonnelli, Supercond. Sci. Technol. **23**, 043001 (2010).
[21] Please note that resistivity measurements unambiguously prove that the film with $x = 0.15$ is in the overdoped region, since (i) its $\rho(T)$ curve does not show the low-temperature upturn typical of underdoped samples (Ref. 18), observed instead in the films with $x = 0.04$ and 0.08 and (ii) its critical temperature is smaller than in the optimally doped film ($x = 0.10$).
[22] R. S. Gonnelli, D. Daghero, G. A. Ummarino, V. A. Stepanov, J. Jun, S. M. Kazakov, and J. Karpinski, Phys. Rev. Lett. **89**, 247004 (2002).
[23] H. Z. Arham, C. R. Hunt, W. K. Park, J. Gillett, S. D. Das, S. E. Sebastian, Z. J. Xu, J. S. Wen, Z. W. Lin, Q. Li *et al.*, Phys. Rev. B **85**, 214515 (2012).
[24] H. Z. Arham, C. R. Hunt, J. Gillett, S. D. Das, S. E. Sebastian, D. Y. Chung, M. G. Kanatzidis, and L. H. Greene, arXiv:1307.1908.
[25] T. Plecenik, M. Gregor, R. Sobota, M. Truchly, L. Satrapinskyy, F. Kurth, B. Holzapfel, K. Iida, P. Kus, and A. Plecenik, Appl. Phys. Lett. **103**, 052601 (2013).
[26] Y. G. Naidyuk and I. K. Yanson, *Point-Contact Spectroscopy*, Springer Series in Solid-State Sciences Vol. 145 (Springer, New York, 2004).
[27] Y. V. Sharvin, Zh. Eksp. Teor. Fiz. **48**, 984 (1965) [Sov. Phys. JETP **21**, 655 (1965)].
[28] G. Wexler, Proc. Phys. Soc. London **89**, 927 (1966).
[29] Y. G. Naidyuk, O. E. Kvitnitskaya, I. K. Yanson, G. Fuchs, S. Haindl, M. Kidszun, L. Schultz, and B. Holzapfel, Supercond. Sci. Technol. **24**, 065010 (2011).
[30] T. Y. Chen, S. X. Huang, and C. L. Chien, Phys. Rev. B **81**, 214444 (2010).
[31] S. Döring, S. Schmidt, S. Gottwals, S. Schmidl, V. Tympel, I. Mönch, F. Kurth, K. Iida, B. Holzapfel *et al.*, arXiv:1309.1641.
[32] D. Daghero, M. Tortello, G. Ummarino, and R. S. Gonnelli, Rep. Prog. Phys. **74**, 124509 (2011).
[33] S. Kashiwaya, Y. Tanaka, M. Koyanagi, and K. Kajimura, Phys. Rev. B **53**, 2667 (1996).
[34] S. Kashiwaya and Y. Tanaka, Rep. Prog. Phys. **63**, 1641 (2000).

[35]D. Daghero, M. Tortello, P. Pecchio, V. A. Stepanov, and R. S. Gonnelli, Low Temp. Phys. **39**, 199 (2013).
[36]R. S. Gonnelli, M. Tortello, D. Daghero, P. Pecchio, S. Galasso, V. A. Stepanov, Z. Bukovski, N. D. Zhigadlo, J. Karpinski, K. Iida *et al.*, J. Supercond. Nov. Magn. **26**, 1331 (2013).
[37]R. S. Gonnelli, D. Daghero, and M. Tortello, Curr. Opin. Solid State Mater. Sci. **17**, 72 (2013).
[38]G. Sheet, M. Mehta, D. A. Dikin, S. Lee, C. Bark, J. Jiang, J. D. Weiss, E. E. Hellstrom, M. S. Rzchowski, C. B. Eom *et al.*, Phys. Rev. Lett. **105**, 167003 (2010).
[39]W. K. Park, C. R. Hunt, H. Z. Arham, Z. J. Xu, J. S. Wen, Z. W. Lin, Q. Li, G. D. Gu, and L. H. Greene, arXiv:1005.0190.
[40]M. Tortello, D. Daghero, G. A. Ummarino, V. A. Stepanov, J. Jiang, J. D. Weiss, E. E. Hellstrom, and R. S. Gonnelli, Phys. Rev. Lett. **105**, 237002 (2010).
[41]We used different barrier parameters for the two bands because of the different Fermi velocities (Ref. 20) since $Z = U_0/(\hbar v_F)$ being U_0 the height of the potential barrier at the interface. Interestingly, in the $x = 0.08$ case where we have the larger statistics, we found that $Z_L/Z_S = v_{F,S}/v_{F,L} = 1.55 \pm 0.40$. This is an indirect way to estimate the ratio of Fermi velocities in the two equivalent bands that host the two gaps Δ_L and Δ_S.
[42]I. I. Mazin, T. P. Devereaux, J. G. Analytis, J.-H. Chu, I. R. Fisher, B. Muschler, and R. Hackl, Phys. Rev. B **82**, 180502(R) (2010).
[43]R. S. Gonnelli, M. Tortello, D. Daghero, R. K. Kremer, Z. Bukovski, N. D. Zhigadlo, and J. Karpinski, Supercond. Sci. Technol. **25**, 065007 (2012).
[44]D. V. Efremov, M. M. Korshunov, O. V. Dolgov, A. A. Golubov, and P. J. Hirschfeld, Phys. Rev. B **84**, 180512(R) (2011).
[45]F. Hardy, P. Burger, T. Wolf, R. A. Fisher, P. Schweiss, P. Adelmann, R. Heid, R. Fromknecht, R. Eder, D. Ernst *et al.*, Europhys. Lett. **91**, 47008 (2010).
[46]P. Samuely, Z. Pribulová, P. Szabó, G. Pristáš, S. L. Bud'ko, and P. C. Canfield, Physica C **469**, 507 (2009).
[47]J. J. Tu, J. Li, W. Liu, A. Punnoose, Y. Gong, Y. H. Ren, L. J. Li, G. H. Cao, Z. A. Xu, and C. C. Homes, Phys. Rev. B **82**, 174509 (2010).
[48]F. Hardy, T. Wolf, R. A. Fisher, R. Eder, P. Schweiss, P. Adelmann, H. v. Löhneysen, and C. Meingast, Phys. Rev. B **81**, 060501(R) (2010).
[49]K. Terashima, Y. Sekiba, J. H. Bowen, K. Nakayama, T. Kawahara, T. Sato, P. Richard, Y.-M. Xu, L. J. Li, G. H. Cao *et al.*, Proc. Natl. Acad. Sci. U.S.A. **106**, 7330 (2009).
[50]Y. Yin, M. Zech, T. L. Williams, X. F. Wang, G. Wu, X. H. Chen, and J. E. Hoffman, Phys. Rev. Lett. **102**, 097002 (2009).
[51]G. A. Ummarino, M. Tortello, D. Daghero, and R. S. Gonnelli, Phys. Rev. B **80**, 172503 (2009).
[52]G. A. Ummarino, Phys. Rev. B **83**, 092508 (2011).
[53]I. I. Mazin, D. J. Singh, M. D. Johannes, and M. H. Du, Phys. Rev. Lett. **101**, 057003 (2008).
[54]G. M. Eliashberg, Sov. Phys. JETP **11**, 696 (1963).
[55]L. Boeri, M. Calandra, I. I. Mazin, O. V. Dolgov, and F. Mauri, Phys. Rev. B **82**, 020506 (2010).
[56]I. I. Mazin and J. Schmalian, Physica C **469**, 614 (2009).
[57]R. Mittal, Y. Su, S. Rols, T. Chatterji, S. L. Chaplot, H. Schober, M. Rotter, D. Johrendt, and T. Brueckel, Phys. Rev. B **78**, 104514 (2008).
[58]P. Popovich, A. V. Boris, O. V. Dolgov, A. A. Golubov, D. L. Sun, C. T. Lin, R. K. Kremer, and B. Keimer, Phys. Rev. Lett. **105**, 027003 (2010).
[59]G. A. Ummarino, D. Daghero, M. Tortello, and R. S. Gonnelli, J. Supercond. Novel Magn. **24**, 247 (2011).
[60]G. A. Ummarino, J. Supercond. Novel Magn. **25**, 1333 (2012).
[61]D. Daghero, M. Tortello, G. Ummarino, V. A. Stepanov, F. Bernardini, M. Tropeano, M. Putti, and R. S. Gonnelli, Supercond. Sci. Technol. **25**, 084012 (2012).
[62]J. Paglione and R. L. Greene, Nat. Phys. **6**, 645 (2010).
[63]I. I. Mazin (private communication).
[64]L. Fang, H. Luo, P. Cheng, Z. Wang, Y. Jia, G. Mu, B. Shen, I. I. Mazin, L. Shan, C. Ren *et al.*, Phys. Rev. B **80**, 140508(R) (2009).
[65]E. van Heumen, Y. Huang, S. de Jong, A. B. Kuzmenko, M. S. Golden, and D. van der Marel, Eur. Phys. Lett. **90**, 37005 (2010).